PNAS RESEARCH ARTICLE | NEUROSCIENCE

A thalamocortical substrate for integrated information via critical synchronous bursting

Brandon R. Munn[a,b,1], Eli J. Müller[a,b], Jaan Aru[c], Christopher J. Whyte[a,b], Albert Gidon[d,e], Matthew E. Larkum[d,e], and James M. Shine[a,b]

Edited by Peter Strick, University of Pittsburgh Brain Institute, Pittsburgh, PA; received May 23, 2023; accepted September 21, 2023

Understanding the neurobiological mechanisms underlying consciousness remains a significant challenge. Recent evidence suggests that the coupling between distal–apical and basal–somatic dendrites in thick-tufted layer 5 pyramidal neurons ($L5_{PN}$), regulated by the nonspecific-projecting thalamus, is crucial for consciousness. Yet, it is uncertain whether this thalamocortical mechanism can support emergent signatures of consciousness, such as integrated information. To address this question, we constructed a biophysical network of dual-compartment thick-tufted $L5_{PN}$, with dendrosomatic coupling controlled by thalamic inputs. Our findings demonstrate that integrated information is maximized when nonspecific thalamic inputs drive the system into a regime of time-varying synchronous bursting. Here, the system exhibits variable spiking dynamics with broad pairwise correlations, supporting the enhanced integrated information. Further, the observed peak in integrated information aligns with criticality signatures and empirically observed layer 5 pyramidal bursting rates. These results suggest that the thalamocortical core of the mammalian brain may be evolutionarily configured to optimize effective information processing, providing a potential neuronal mechanism that integrates microscale theories with macroscale signatures of consciousness.

integrated information | dendrites | biophysical network | synchronous bursting | nonspecific thalamus

Significance

Consciousness emerges from intricate neuronal interactions, yet the underlying mechanisms remain unclear. Recent studies highlight thalamic gating of nonlinear layer 5 pyramidal cells as crucial for consciousness. By exploring neuronal simulations with varying thalamic input, we reveal that diffuse thalamic projections nonlinearly regulate integrated information, a key signature of conscious awareness. Our findings demonstrate a convergence of maximal integrated information with correlated neuronal variability and criticality signatures. That is to say, coordinated and variable neuronal spiking optimizes information processing. These findings reveal the neuronal mechanisms supporting consciousness, highlighting the interplay between thalamic modulation, integrated information, criticality, and efficient information processing in the brain.

Multiple leading theories of consciousness, including global neuronal workspace theory and integrated information theory, implicate the integration of corticocortical and thalamocortical systems in conscious awareness (1–3). Although these theories differ on critical anatomical areas for awareness, both agree that conscious awareness is supported by neural activity with high informational capacity. This process is highly dynamic changing across states of arousal (e.g., anesthesia and wake), and it has been linked to a critical process controllably emerging near a phase transitions critical point (4–6). Neurobiologically, this information processing is thought to involve the integration of separate information streams across a broad thalamocortical network that includes both specific (a.k.a. "core" or "first-order"; Fig. 1*A*, blue) and nonspecific thalamocortical circuits (a.k.a. "matrix" or "higher-order"; Fig. 1*A*) (1, 2, 7–15). To date, these hypotheses remain primarily theoretical.

Most evidence informing current theories of consciousness comes from noninvasive whole-brain neuroimaging techniques. Numerous macroscopic measures have been proposed to signify alterations in conscious awareness (7) that quantify combinations of integration and information. A prominent measure is Φ, which quantifies the information that is integrated by the complex interactions within the components of the system (16)—i.e., the extent that the whole is greater than the set of its parts (17). Φ has been related to different states of consciousness in macroscale electrophysiological recordings (16). Despite theoretical import, the underlying neuronal processes that support consciousness are not directly measurable at the macroscopic scale, and as such, we lack a mechanistic understanding of the neuronal drivers of these phenomena (1, 7).

The Dendritic Integration Theory (DIT) (18, 19) of consciousness bridges the gap between systems-level theories and neurobiological mechanisms. Using insights from microscopic neurobiology, DIT proposes that conscious awareness depends on the functional integration of diverse streams of cortical and subcortical information that impinge at differential regions of thick-tufted layer 5 pyramidal neurons ($L5_{PN}$) dendrites (Fig. 1*B*) (18). $L5_{PN}$ possess a long apical trunk that physically and electrotonically separates the distal regions of the apical dendrites from the proximal-somatic dendrites (basal) (20, 21). These cells reside at a critical nexus of information flow in the cerebral cortex, as basal dendritic input reflects exogenous sensory-driven feedforward activity, whereas apical input reflects endogenous higher-cortical contextual feedback activity. Remarkably, $L5_{PN}$ can display nonlinear sequences of action-potentials ("spikes"). The apical dendrites can generate a calcium spike that if exceeding the apical–basal electrotonic separation and

Author contributions: B.R.M., M.E.L., and J.M.S. designed research; B.R.M. performed research; B.R.M. contributed new reagents/analytic tools; B.R.M. analyzed data; and B.R.M., E.J.M., J.A., C.J.W., A.G., M.E.L., and J.M.S. wrote the paper.

The authors declare no competing interest.

This article is a PNAS Direct Submission.

[1]To whom correspondence may be addressed. Email: brandon.munn@sydney.edu.au.

Published November 8, 2023.

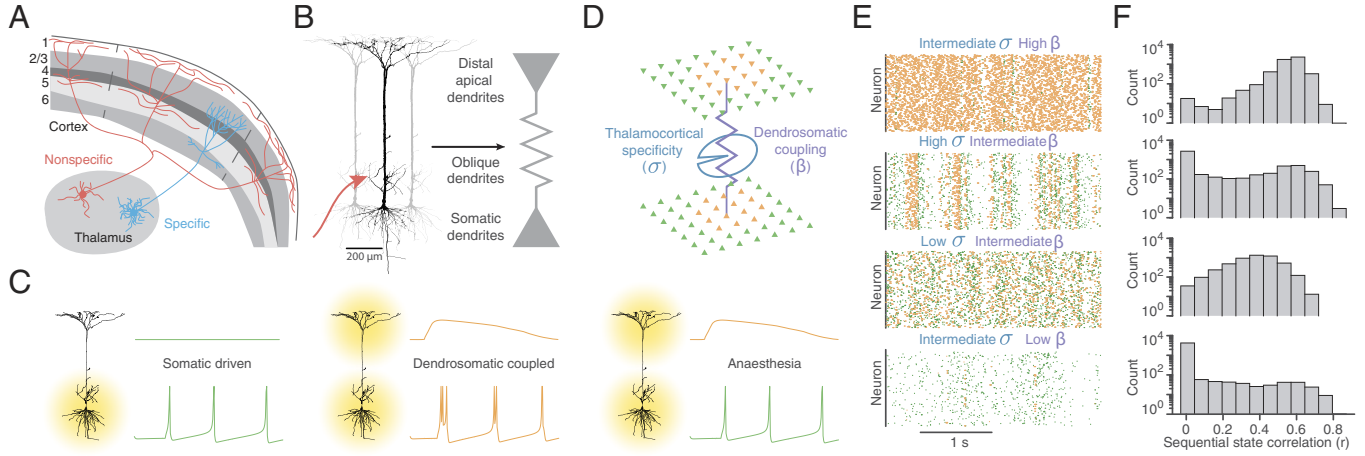

Fig. 1. Connecting macroscopic measures of consciousness with microscale computational modeling. (*A*) Many theories and empirical findings agree that conscious awareness is supported by thalamocortical and corticocortical interactions producing integrated neuronal activity with a large informational capacity at the whole-brain scale. This interaction has been linked with the broadly projecting nonspecific thalamus (red) and not the targeted projections of the specific thalamus (blue); (*B*) Thick-tufted layer 5 pyramidal neurons ($L5_{PN}$) possess two dendritic compartments, the supragranular distal apical dendrites, which predominantly receive corticocortical feedback, and the infragranular proximal somatic dendrites (basal), which predominantly receive corticocortical feedforward and specific thalamocortical input. The oblique dendrites along the apical trunk targeted by the nonspecific thalamus (red arrow) control the dendrosomatic coupling between the apical and basal compartments. (*C*) Basal dendritic drive leads to regular spiking (green; *Left*), and when dendrosomatic coupled, coincident apical drive and somatic sodium spikes can transition the cell into high-frequency bursting (orange; *Middle*). (*Right*) However, when the apical and basal dendrites are decoupled (e.g., under anesthesia), even with basal and apical input the cell does not transition from spiking to bursting. (*D*) We created a network of $L5_{PN}$ modeled as two separate dendritic compartments (apical and basal) that were coupled via dendrosomatic coupling term (β–purple) that received thalamocortical input with a spatiotemporal specificity (σ–navy). (*E*) Changing these parameters leads to qualitatively different spike (green) and burst (yellow) dynamical regimes in simulations with identical somatic drive. (*F*) The coincidence of sequential activity states (i.e., coactive "ensembles" of neurons) similarly varied across the parameter regime. Here, long-lasting ensembles of neurons possess a large Pearson correlation (r) and vice versa for short-lived ensembles.

coincident with somatic sodium spikes (Fig. 1*C*, green) can transition into high-frequency spiking ("bursting"; Fig. 1*C*, orange). As such, $L5_{PN}$ bursting can signal and amplify the communication of the match between feedforward and feedback activity (22). Importantly, $L5_{PN}$ bursting has been linked to changes in the state [i.e., anesthesia prevents $L5_{PN}$ bursting (23)] and contents [i.e., $L5_{PN}$ bursting is concomitant with perceived stimuli (24)] of consciousness.

The thalamus is a pivotal structure in many theories of consciousness (3, 12, 18, 25, 26) and plays a crucial role in linking the apical and basal compartments of thick-tufted $L5_{PN}$. Specifically, recent empirical evidence has demonstrated that nonspecific thalamocortical input targets the oblique dendrites along the apical trunk of $L5_{PN}$ (Fig. 1*B*, red arrow) and, in turn, gates dendrosomatic coupling via the activation of metabotropic glutamate receptors (23, 27, 28). In this experiment, input into the apical dendrites of $L5_{PN}$ capable of eliciting somatic bursting was suppressed with anesthesia and the inactivation of the nonspecific thalamus (Fig. 1 *C*, *Right*) (23). The nonspecific thalamus broadly projects to the cortex, unlike specific thalamocortical input to the granular layers with precise projections along sensory pathways (15, 25, 29). Furthermore, electrical stimulation of the nonspecific thalamus restores consciousness in anesthetized primates (30, 31). Based on these empirical results, we hypothesize that the dendrosomatic coupling between apical and basal compartments of $L5_{PN}$ mediated by the nonspecific thalamus in a network of neurons effectively increases integrated information and the capacity to support conscious awareness (18).

The testing of this hypothesis has thus far been empirically prohibitive. Technological challenges currently limit our ability to precisely record a substantial number of thick-tufted $L5_{PN}$. Testing this hypothesis requires precise recordings from the apical and basal dendrites and nonspecific thalamus. In previous work, we have argued that computational modeling is ideally placed to solve this problem and navigate between macroscopic and microscopic scales (32). Perhaps unsurprisingly, appropriately capturing the complexity of the nonlinear spiking of $L5_{PN}$ is a nontrivial problem (20, 33). Existing $L5_{PN}$ models capture numerous features of their inherent complexity and, in turn, output realistic spiking properties that match the system's critical features (33, 34). However, these models contain a multitude of differential equations that ultimately limit their capacity to isolate factors and simulate large-scale networks and thus extrapolate from microscopic features to macroscopic principles.

Results

We created a biophysical model ($N \times N$ network of Izhikevich neurons on a torus $N = 70$; see *Methods*) that isolated the role of the oblique dendritic thalamocortical nexus between the apical and basal dendrites of thick-tufted $L5_{PN}$. Specifically, we created a model of $L5_{PN}$ with asynchronous regular spiking when driven by the basal dendrites (35) that could transition into a biophysically matched unique high-frequency spiking (bursting) mode dependent on coincident apical dendritic activity exceeding the dendrosomatic coupling (β) gated by thalamocortical inputs (Fig. 1*D*). β is normalized to map directly to the bursting ratio – i.e., when $\beta = 0$ all action potentials are low-frequency spikes (Fig. 1 *E*, *Bottom* row) and when $\beta = 1$ all spikes are high-frequency bursts (Fig. 1 *E*, *Top*-row). Inputs to the apical and basal compartments were modeled as white noise, approximating a barrage of desynchronized postsynaptic potentials (36, 37), and the network is poised in a balanced excitatory/inhibitory regime. Bursting increases the likelihood of neuronal "ensembles" (correlated neuronal coactivation patterns) within the network via an enhancement of neuronal coupling, as an afferent burst is far more likely to elicit an efferent action potential than an afferent spike. Ensembles are detected by contrasting the correlation in sequential spiking patterns (*Methods*). The ensemble consistency transitions from predominantly asynchronous activity (i.e., no coordinated

ensembles; Fig. 1 *F*, *Bottom* row) to repeatedly correlated patterns (Fig. 1 *F*, *Top* row; $P < 10^{-16}$ Two-sample Kolmogorov–Smirnov test). Our model of $L5_{PN}$ captures the critical feature of their functional neuroanatomy—namely, empirically matched burst-firing dependent on apical input, dendrosomatic coupling, and coincident somatic spiking (32, 38).

Synchronous Bursting Via the Nonspecific Thalamus Maximizes Integrated Information. With the network of Izhikevich neurons capable of biophysically matched $L5_{PN}$ spiking and bursting (39), we asked whether increasing dendrosomatic coupling in a population of reciprocally connected $L5_{PN}$ would trigger network-wide increases in integrated information (i.e., Φ). Φ is an attempt to quantify the increase in information generated by a system as a whole above and beyond its parts.

Due to the computational challenges associated with directly calculating Φ, we subsampled neuronal activity in our model (169 neurons per subsampling repeated 100 times; see *Methods* for calculation) and calculated Φ* (utilizing mismatched decoding as a measure of integrated information (Fig. 2*A*) (16)) on the neuronal firing rate. The state X^t is defined as the spikes binned into 1 ms nonoverlapping windows. Φ* quantifies how well the past state ($X^{t-\tau}$) of a system can be predicted from the current state $I(X^t; X^{t-\tau})$. It contrasts how informative the current state is (Fig. 2*A*, orange), against assuming the parts were independent $I^*\left(X^t; X^{t-\tau}\right)$ (Fig. 2*A*, green) (16). The difference between these two measures defines $\Phi^* = I\left(X^t; X^{t-\tau}\right) - I^*(X^t; X^{t-\tau})$, and it is the amount of loss of information due to the disconnection between two or more variables. Large values of Φ* imply that the current state had more integrated information than the sum of its (disconnected) parts (16). We present results for the "atomic partition" (Fig. 2*A*, green), whereby all neurons are assumed to be independent, and we present results for a temporal lag of $\tau = 1$ ms (i.e., the previous timestep), as Φ* was maximal at this lag (results are consistent for lags of $\tau = 1$ to 50 ms).

We found that asynchronously increasing the dendrosomatic coupling between apical and basal compartments (via stimulating $L5_{PN}$ oblique dendrites) led to a nonmonotonic increase in Φ* (Fig. 2*B*, blue; error-bars are SEM across 50 subsamples). This relationship confirms our hypothesis that apical–basal dendrosomatic coupling can reproduce key correlates of conscious awareness as predicted by DIT.

How might the physical anatomy of thalamocortical projections further enhance this dendrosomatic coupling and hence augment information integration in the brain? The thalamocortical neurons that innervate the oblique dendrites of $L5_{PN}$ in layer 5A of the cerebral cortex are nonspecific—i.e., their axons often diverge to cover multiple cortical areas (Fig. 1*A*, red) (23, 25). We wondered whether introducing the nonspecific thalamus (29, 40) to coordinate dendrosomatic coupling spatially between reciprocally connected $L5_{PN}$ would enhance Φ*. To explore this anatomical feature, we introduced dendrosomatic coupling among reciprocally connected $L5_{PN}$ via nonspecific thalamocortical inputs (σ; Fig. 1*D*). σ represents the SD of the spatial coordination of thalamocortical specificity. For example, $\sigma = 0$ neurons are thalamocortically coupled independent of physical connections resulting in asynchronous bursts (Fig. 1*E*, third-row) and intermediately persistent neuronal ensembles (Fig. 1*F*, third-row). Whereas for increasing σ up to $\sigma = N$, all neurons are simultaneously coupled as if driven by highly nonspecific thalamic population, and bursts are synchronous (Fig. 1*E*, second-row). This synchrony results in transient ensembles with variance an order of magnitude larger than other regimes (variance ~ 0.1; Fig. 1*F*, second-row). That is to say, variable and synchronous ($\beta \sim 0.5$; $\sigma \sim N$) bursting results in a blend of short- and long-lived neuronal ensembles.

We observed a nonlinear augmentation of Φ* with maximal nonspecific thalamocortical drive (Fig. 2*B*, red; error bars are SEM across 50 subsamples). Specifically, we found that the maximal value of Φ* increases with thalamocortical nonspecificity and occurs at gradually decreasing dendrosomatic coupling (Fig. 2*C*). The largest Φ* occurs when the synchronous bursts are discriminable from the regular spiking background (i.e., an admixture of bursting atop regular spiking; $\beta \sim 0.3$; Fig. 2*B*). This result occurs as the system returns to asynchronous bursting (spiking) at maximal (minimal) dendrosomatic coupling. Only with an admixture of bursts and spikes is the emergent integration from the nonspecific thalamus observed. Interestingly, this maximal Φ* coincides with burst/spike ratios observed empirically (22). Thus, our results demonstrate that the physical structure of nonspecific thalamocortical projections and their dendrosomatic coupling can enhance neuronal integrated information.

Underlying Neuronal Dynamics Supporting Maximal Integrated Information. We wondered how the underlying neuronal spiking supports the increased integrated information. To address this, we calculated two standard neuronal measures, each neuron's average firing rate ($\overline{\rho}$) and firing rate pairwise Pearson correlation $\left(r_{\overline{\rho}}\right)$, and investigated the mean ($\langle X \rangle$) and variance ($V(X) = \left\langle X^2 \right\rangle - \langle X \rangle^2$). We found that mean firing rate, $\langle \overline{\rho} \rangle$, was uncorrelated with Φ* ($r = 0.01$ & $P = 0.9$ Pearson correlation and *P*-value; Fig. 3*A*). This finding is consistent with the minimal effect of anesthesia altering direct neuronal firing rate on consciousness (41). Thus, while we found a firing rate correlation for asynchronous coupling (Fig. 2*B*, blue), this was mediated by the increased informational capacity of faster spiking cells. However, the broad increase in integrated information from the nonspecific thalamus offsets this firing rate

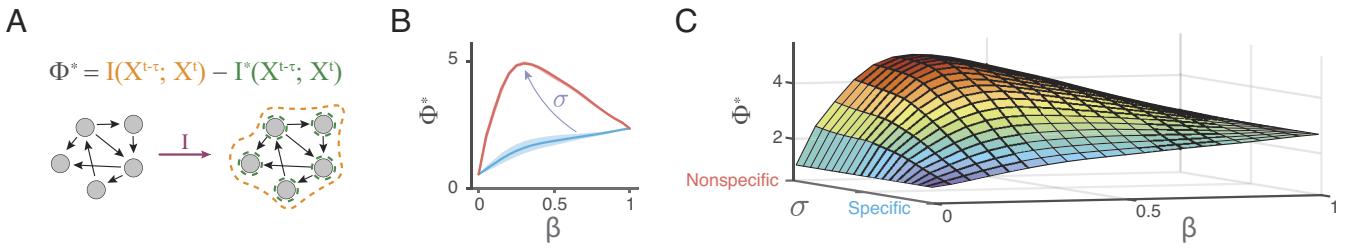

Fig. 2. Thalamocortically controlled $L5_{PN}$ bursting maximizes integrated information. (*A*) Φ* was estimated by calculating the mutual information (*I*, orange) of the past state ($X^{t-\tau}$, orange) given the current state as a whole (X^t, orange and orange dotted lines) and then subtracting the mutual information (*I**, green) of the past state ($X^{t-\tau}$, green), assuming all regions were acting independently (X^t, green and green dotted lines). Adapted from ref. 16. Φ* is high when the whole state is more predictable than the sum of its parts. (*B*) Increasing the burst-firing of $L5_{PN}$ by incrementally asynchronously boosting apical–basal dendrosomatic coupling caused a monotonic increase in integrated information (Φ*; blue line). Whereas, increasing dendrosomatic coupling synchronously caused a nonmonotonic divergence in Φ* (red line). Error bars are 1.96 SEM across 100 subsamples. (*C*) Sweeping the thalamocortical nonspecificity (σ) produced a divergent increase in Φ* due to increased synchronous bursting.

correlation (Fig. 2*B*, red). In contrast, we found that the neurons displayed a broad variability ($V(\bar{\rho})$) in neuronal spiking activity, with a maximum alignment associated with the same parameter combination associated with a peak in Φ^* ($r = 0.7$ & $P < 1 \times 10^{-16}$; Fig. 2*B*). Unsurprisingly, these univariate measures were unaffected by σ and changed with β.

We next wondered how pairwise measures were modified by nonspecific thalamocortical dendrosomatic coupling. To this end, we calculated all neuronal pairwise firing rate Pearson's correlations and found that the mean $\langle r_{\bar{\rho}} \rangle$ was small ($\langle r_{\bar{\rho}} \rangle < 0.15$ due to the excitatory/inhibitory balanced-state (42)) and strongly correlated with Φ^* ($r = 0.9$ & $P < 1 \times 10^{-16}$; Fig. 3*C*). As the network is in a balanced E:I connectivity regime, neuronal activity is asynchronous when either only regular spiking ($\beta \sim 0$) or maximally bursting ($\beta \sim 1$), and that the increase in correlations via synchronous bursting ($\sigma \to N$) is maximal for intermediate coupling. That is to say, the nonspecific thalamocortical mediated synchronous bursts are only capable of altering neuronal correlations when the system is not inundated with bursting. Furthermore, this maximal peak in integrated information was also reflected in a diversity of correlations ($r = 0.41$ & $P < 1 \times 10^{-16}$; Fig. 3*D*). That is to say, the integrated information is strongly related to an increase in neuronal coordination (Fig. 3*C*), but not pure synchrony reflected by the diverse spiking activity (Fig. 3*B*) and coordination (Fig. 3*D*).

Integrated Information Aligns with Optimal Signatures of Criticality and Communication. Beyond integrated information, various other theories of the brain have argued that consciousness would be supported by the beneficial properties of being poised near the critical point (5, 6). A system poised at a critical point displays long-range correlations, a maximal susceptibility to external stimuli, a broad variability in coordinated states, and information transmission (43, 44)—all of which are putative benefits of conscious awareness. Our model, therefore, represents a unique opportunity to formally relate these measures to one another.

To this end, we calculated three criticality measures (spatial correlation decay, susceptibility, and metastability) and a network communication measure (communicability). As the model is spatially embedded, we calculated the decay rate of correlations, ξ, with distance by fitting an exponential decay $r(d) = e^{-\frac{d}{\xi}}$, with spatial distance d (45). The spatial correlation is a signature of criticality as at the critical point, the spatial correlation diverges (43). We observe evidence of the spatial decay extending beyond the range of reciprocal connections at maximal Φ^* (Fig. 4 *A*, *Left*). Susceptibility, $\chi_\rho = N\left(\langle \rho_S^2 \rangle - \langle \rho_S \rangle^2\right)$ where $\rho_S = \frac{1}{N}\sum_i \rho_i$ is the population spiking activity order parameter (46). Susceptibility characterizes the optimal receptivity to external input (Fig. 4 *B*, *Left*). Metastability $x_\theta = N\left(\langle \theta^2 \rangle - \langle \theta \rangle^2\right)$ where $\theta = \frac{1}{N}\sum_i e^{i\theta_i}$ is the phase alignment order parameter between each neuron (θ_i estimated from the firing rate using the Hilbert transform), which ranges between zero (when the phases of each neuron's firing rate are uniformly distributed) and one (when all neurons are in phase). Metastability captures the temporal variability of neuronal ensembles activity coherence (Fig. 4 *C*, *Left*) (47). Finally, communicability, $C = \frac{1}{N^2}\sum_{i,j} e^{W_{i,j}}$, where $W_{i,j}$ is the normalized weighted connectivity matrix estimated using the functional connectivity $W_{i,j} = r_{i,j} / \left(\sqrt{r_i}\sqrt{r_j}\right)$ from the neuronal pairwise correlation matrix $r_{i,j}$ and the neuron strength $\sqrt{r_i} = \sum_j r_{i,j}$. Communicability quantifies the communication across a functional neuronal network via diffusive broadcasting (i.e., communication follows all possible paths between neurons; Fig. 4 *C*, *Left*) (48, 49).

Consistent with the deep links between criticality, information processing, and consciousness (5), all four measures were tightly correlated with Φ^* (Fig. 4 *A*–*D*, *Right*). Spatial correlation decay ($r = 0.85$ & $P < 1 \times 10^{-16}$; Fig. 4 *A*, *Right*) and system susceptibility ($r = 0.91$ & $P < 1 \times 10^{-16}$; Fig. 4 *B*, *right*) strongly align to Φ^*, whereas metastability is maximized at a slightly higher dendrosomatic coupling ($r = 0.76$ & $P < 1 \times 10^{-16}$; Fig. 4 *C*, *Right*), indicating that Φ^* is peaked in a slightly subcritical synchronous regime (50). Further, we found that maximal C strongly aligns with the peak in Φ^* ($r = 0.9$ & $P < 1 \times 10^{-16}$; Fig. 4 *D*, *Right*), suggesting that maximal integrated information is supported by optimal neuronal communicability via transient nonspecific thalamocortical coupling (low-intermediate β and high σ). That is to say, the nonspecific thalamus can constrain the higher-order network connectivity and receptivity to stimuli. These signatures are maximized at nonspecific low–intermediate dendrosomatic coupling, again consistent with the observed increase in Φ^* and leading theories of consciousness (19, 28, 51). Finally, we found that integrated information is significantly explained by increases in signal susceptibility and communicability (both explained variance > 80%).

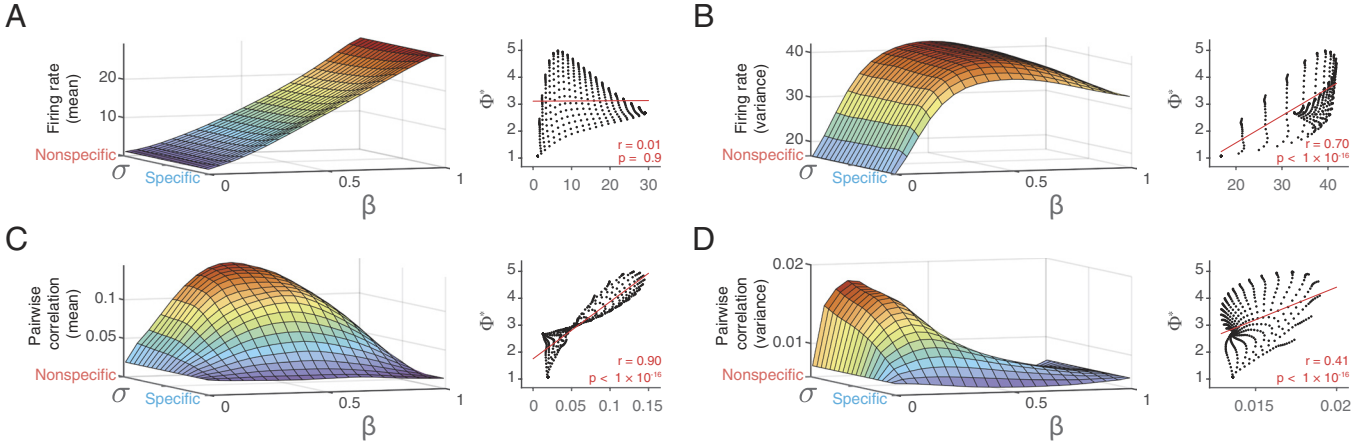

Fig. 3. The role of neuronal spiking dynamics and coordination in the augmentation of information integration. The neuronal firing rate distribution mean (*A*) and variance (*B*) across model properties (β & σ). The correlation across the model state-space and integrated information (Φ^*). Same as in (*A* and *B*) for the pairwise correlation distribution mean (*C*) and variance (*D*). Least-squares regression in red.

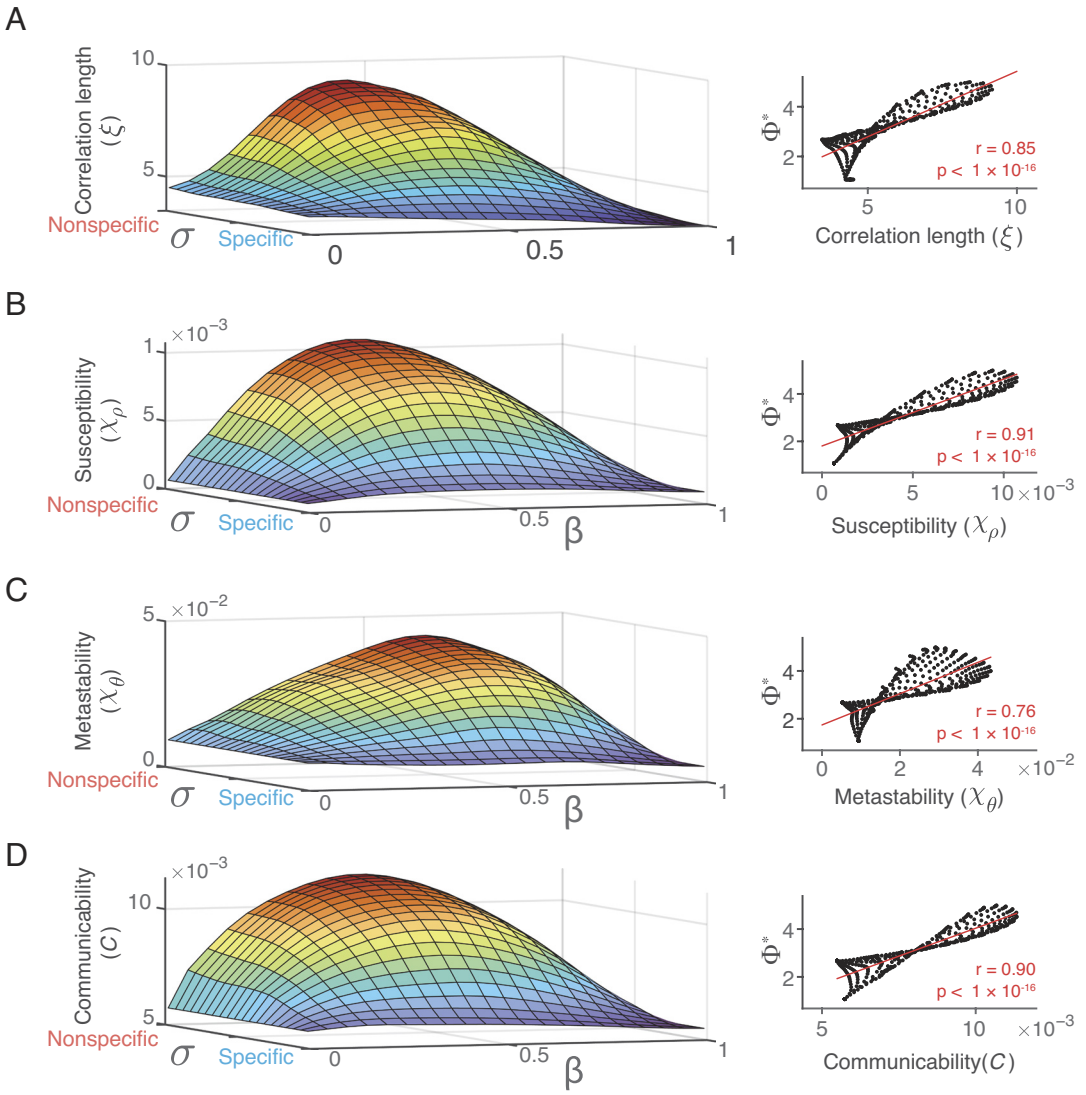

Fig. 4. Signatures of criticality and information communication coincide with integrated information. (*Left*) Signatures of criticality (*A*) Spatial correlation length, ξ, (*B*) susceptibility, χ_ρ, (*C*) metastability, χ_θ, and (*D*) neuronal network communicability, *C*, across the model state-space. (*Right*) Correlation with integrated information Φ*. Least-squares regression in red.

Discussion

These results of our biophysical model suggest a plausible implementation for conscious awareness in the mammalian brain—namely, the nonspecific thalamic gated dendrosomatic coupling of thick-tufted $L5_{PN}$ (Fig. 1). The coordination of the three dendritic regions—somatic, apical, and oblique dendrites—within networks of $L5_{PN}$ was sufficient to mediate an increase in integrated information Φ* (16) (Fig. 2). The maximal observed Φ* occurred with a synchronous coupling that maximized pairwise neuronal correlations and neuronal firing rate diversity (Fig. 3). Further, this regime supports optimal signatures of criticality and communication due to patterns of spatiotemporally coordinated burst firing (Fig. 4). These theoretical results reconcile disparate empirical findings, such as anesthetic decoupling of the apical and basal dendrites of $L5_{PN}$ (18) and the recovery of awake behavior following stimulation of nonspecific thalamus (30, 31), and further lead to testable predictions for changes in neuronal spiking properties and spatiotemporal bursting dynamics.

Coordinated $L5_{PN}$ bursting represents a parsimonious correlate of awareness across various theories of consciousness (18, 19, 28). The results of this study are a natural application of Dendritic Information Theory (18, 19), where the coupling of apical and basal compartments of $L5_{PN}$ provided a mechanistic implementation for a phenomenal conscious experience. As all levels of cortical hierarchy have principally the same architecture with respect to $L5_{PN}$ and their interaction with the thalamus, both phenomenal consciousness—presumably related to posterior sensory areas (1)—and access consciousness—related to prefrontal areas (26)—are supported through the same mechanism. In addition, many scholars have argued that the brain exploits critical dynamics, and we find alignment across various signatures of criticality and integrated information supporting the critical brain hypothesis (5). Further, the global–neuronal workspace theory of consciousness (26, 51) proposes that a consciously perceived stimulus must pass an initial threshold, leading to an ignition into the neuronal workspace. Our results suggest that in the maximal Φ* regime, the admixture of bursts and spikes leads the system into a maximally responsive and susceptible state with rich information and communication of neuronal spiking (Fig. 4), all of which have been suggested as relevant for the integrated information theory of consciousness (1, 52, 53). Our theoretical analysis demonstrates a neuronal mechanism by which systems-level signatures of consciousness can emerge in thick-tufted $L5_{PN}$ and emphasizes the essential role of the thalamus in mediating consciousness. As such our findings are consistent with many theories of consciousness

that outline the role of information, integration, and the thalamus (1, 3, 12, 18, 22, 23, 31, 54).

An inherent limitation of our model is that the three dendritic regions (apical, basal, and oblique) have biological interdependencies not incorporated within our model. For example, basal dendritic spiking can elicit back-propagating action potentials distally along the apical trunk, adding to apical dendritic input (21). Another example is that the nonspecific thalamus also synapses on the apical dendrites (23). Thus, the thalamus is poised to increase apical and basal coupling and enact upon the coupling forming cortico-thalamocortical loops that enhance apical–basal coupling (18, 27, 55). Further, various other mechanisms can modify the likelihood of thick-tufted $L5_{PN}$ bursting that have not been considered, such as adrenergic (56) and cholinergic (23) neuromodulation (57) or ephaptic changes in subthreshold dendritic voltages (58). Nevertheless, this simplified model captures the core concept of these biological implementations: demonstrating the benefits of coordinated dynamic switching between regular and high-frequency spiking (bursting). Future modeling studies can be readily devised to investigate these details and their implications for consciousness.

In conclusion, these features represent a functional microscale neuronal explanation for systems-level signatures of conscious awareness in the mammalian brain. Our findings indicate that the ability to transiently alter neuronal coupling from spiking to coordinated and synchronous high-frequency bursting generates a spectrum of time-varying neuronal ensembles, spanning asynchronous to repetitively coactive neurons. These dynamic neuronal ensembles facilitate maximal signatures of criticality and integrated information and thus could constitute a neural correlate of consciousness.

Methods

Thick-Tufted $L5_{PN}$ Network Model. The results in the main text were obtained via numerical simulation using a phenomenological quadratic adaptive integrate and fire neuronal model (34), which is a canonical reduced form of Hodgkin–Huxley neuronal dynamics (34), conserving key aspects of their original dynamics (i.e., spike generation and bursting) in a two-dimensional system of ODEs, with four dimensionless parameters that can be modified to recapitulate a range of spike adaptation dynamics that have been observed experimentally. Within the model, the somatic dendritic compartment determines the generation of the spike waveform and dynamics. The interaction between the apical dendritic compartments and the dendrosomatic coupling shifts the spike adaptation of the somatic dynamics between a mode of regular spikes and one of bursting.

First, we define the dynamics of the somatic compartment which generates the spikes. The somatic basal dendritic compartment was modeled by the membrane equation,

$$\frac{dv}{dt} = h\left(0.04v^2 + 5v - u + I\right),$$

$$\frac{du}{dt} = h\left(a\left(bv - u\right)\right),$$

with the after-spike resetting given by

$$\text{if} v \geq 30, \left\{v \leftarrow c(t),\ \ u \leftarrow u + d(t)\right\},$$

where v and u are dimensionless in a form such that the membrane potential, v, and time, t, match empirical spike traces in millivolts and milliseconds (ms), respectively (59, 60). v_r is the resting potential, and u is the recovery variable, defined as the difference between all inward and outward voltage-gated currents [this emulates the activation (inactivation) of potassium (sodium) ionic currents]. I is the input into the somatic dendrites from all presynaptic sources and external drive, and h is the somatic voltage integration step, which was set at 0.5 ms for the membrane potential and 1 ms for the recovery variable to obtain an optimal balance between computational efficiency and accuracy when simulating Izhikevich neurons with Euler integration (61–63).

The parameter a represents the time constant of the spike adaptation current and is set as $a = 0.02$. The parameter b describes the coupling of the adaptation current (u) to subthreshold fluctuations of the membrane potential (v) and is set as $b = 0.02$, when $b > 0$ (<0), it acts as an amplifier (resonator). These parameters and the constants are set to biophysically match the spike properties to experimentally observed $L5_{PN}$ activity (see ref. 59 for further details). The parameters c and d represent the after-spike reset of v and u, controlling the voltage reset to model the effect of fast high-threshold K+ conductances and the slow high-threshold Na+ and K+ conductances activated during the spike similarly modulating spike adaptation as a, respectively. The parameters c and d are time-varying and are modified by the dendrosomatic coupling, as detailed below.

In this paper, we studied a recurrent network of $L5_{PN}$. The network consisted of $N = 70 \times 70 = 4{,}900$ neurons with a toroidal grid topology (10 μm spacing; 70 × 70) where afferent connections were made between neurons falling within a somatic dendritic tree radius of 200 μm (64). Total synaptic currents, I, into the somatic dendrites, is prescribed by $I = I_{ext} + s$, where I_{ext} represents the external input to the $L5_{PN,}$ such as lower-cortical feedforward and subcortical structures. This parameter was modeled as white noise ($\mu_{I_{ext}} = 0$ mV, $\sigma_{I_{ext}} = 5$ mV) to induce spontaneous activity (2 Hz mean firing rate). For a given neuron i, s_i represents the synaptic input from all afferent neurons. We utilized homogenous network connectivity utilizing a sum of two exponentials (i.e., Mexican-hat coupling) to model the local excitation and lateral inhibition effects with a current-based approach over conductance for computational efficiency (65). The total synaptic input into a neuron, i, is then given by $s_i(t) = \sum_j \sum_k w_{ij}\ \delta\left(t - t_j^k\right)$, where δ is the Kronecker delta function and spikes at time t^k from all afferent neurons, j, are scaled by a synaptic coupling weight, w_{ij}, and summed. The synaptic coupling strength follows a difference of Gaussians or "Mexican-hat" function which recapitulates $L5_{PN}$ connectivity profiles (65) given by

$$w_{ij} = \left\{ \begin{array}{c} 0 \text{ if } d_{ij} > d_{max} \text{ or } i = j \\ C_E e^{-\frac{d_{ij}^2}{d_E}} + C_I e^{-\frac{d_{ij}^2}{d_I}}, \text{ if } 0 < d_{ij} < d_{max} \end{array} \right\},$$

where d_{ij} is the geodesic distance between neuron i and j, $C_E = 21.5$ and $C_I = C_E / 2$ are the excitatory and inhibitory coupling constants, and $d_E = 10$ and $d_I = d_{max} = 20$ are the excitatory and inhibitory coupling ranges, respectively. The parameters used in the model are set such that the network is balanced, defined as $\sum w_{ij} = 0$, i.e., the net synaptic coupling into each neuron is zero.

The somatic dendritic compartment of each neuron was coupled to its corresponding apical dendritic compartment could transition the somatic dendritic compartment from a regular spiking mode to a burst spiking model (36), depending upon the apical activity and the dendrosomatic coupling mediated by diffusely projecting thalamus targeting oblique dendrites. The apical compartment activity, $\alpha_i(t)$, was modeled as receiving normalized white noise drive ($\mu = 0,\ \ \sigma = 1$) that was integrated over the previous 25 ms (66) and mapped to spatial correlation by convolving activity with a Gaussian kernel, $G_\sigma\left(d_{ij}\right) = \frac{1}{2\pi\sigma^2} e^{-\frac{\left|d_{ij}\right|^2}{2\sigma^2}}$. The dendrosomatic coupling of the apical and basal compartments controls the neuronal spiking variables $c_i(t)$ and $d_i(t)$, following

$$c_i(t) \ = \ -65 + 10H\left(\sum_{t'=t-25}^{t} \alpha_i(t') - I_h(\beta, \sigma)\right), \ \&,$$

$$d_i(t) = 8 - 4H\left(\sum_{t'=t-25}^{t} \alpha_i(t') - I_h(\beta, \sigma)\right),$$

with H as the Heaviside step function and I_h as the electrotonic leak-current, a function of the apical–basal dendrosomatic coupling β and thalamocortical

specificity σ. This results in two conditions: If the apical activity does not exceed the electrotonic separation, then $c = -65$ and $d = 8$, and the neuron recapitulates regular spiking dynamics, such that when driven with constant input, the neuron responds with a short interspike interval (ISI) which gradually increases with input amplitude; in contrast, if the apical current exceeds the electrotonic leak-current, then, $c = -55$ and $d = 4$, which recapitulates intrinsically bursting spike dynamics, such that when driven with constant input, the neuron responds with bursting, followed by repetitive short ISI spikes (67). In the manuscript, we present results from $I_h(\beta = 0) = -3$ to $I_h(\beta = 1) = 3$ in 20 linear steps, and σ ranging from $I_h(\sigma = 1)$ spatially uncorrelated coupling to $I_h(\sigma = N)$ spatially correlated coupling in 42 linear steps. Thus, we ran $40 \times 42 = 1{,}680$ simulations, with identical temporal drive and apical input, prior to Gaussian convolution. We ran each simulation for 35 s, in timesteps of $\Delta t = 0.5$ ms and discarded the initial 15 s of simulation to avoid transient dynamics induced by initial conditions. The parameters were chosen based on original research that fit the spike profiles of regular spiking and bursting $L5_{PN}$ (34).

Integrated Information. Integrated information, Φ, is defined theoretically as the amount of information a system generates as a whole, above and beyond the amount of information its parts independently generate (1). Due to the complexity of the system and the large number of simultaneous activities analyzed, the calculation of integrated information is typically considered computationally intractable. Thus, we utilized an approximated measure, Φ^*, calculated through mismatched decoding developed from information theory; see ref. 16 for a complete derivation of the method. Furthermore, we were still required to decrease the system's variables and thus calculated the measure across repeated stochastic subsamples (68) of the neuronal activity (X^t) into 169 neurons repeated 100 times, and the mean Φ^* is presented. Briefly, $\Phi^* = I - I^*$, where I is the mutual information $I\left(X^{t-\tau} \mid X^t\right) = H\left(X^{t-\tau}\right) - H\left(X^{t-\tau} \mid X^t\right)$, with $H\left(X^{t-\tau}\right)$ the entropy of the past states and $H\left(X^{t-\tau} \mid X^t\right)$ the conditional entropy of the past states given the current state has about its past–at a time lag of $\tau = 1$ ms, and I^* (disconnected I) is the mismatched information that cannot be partitioned into independent parts. These are estimated by contrasting the full conditional probability distribution of activity, $p\left(X^t \mid X^{t-\tau}\right) = p(M_1^t, \cdots M_m^t \mid M_1^{t-\tau}, \cdots M_m^{t-\tau})$ across M parts of the system against a mismatched partitioning $q\left(X^t \mid X^{t-\tau}\right) = \Pi_{i=1}^{m} p\left(M_i^t \mid M_j^{t-\tau}\right)$, where a system is partitioned into parts and the parts M_i are assumed to be independent. For our analysis, we considered the most straightforward partition scheme, the atomic partition, in which Φ^* is calculated assuming each neuron is independent. In this sense, the 'atomic partition' gives the upper bound of Φ because it quantifies the amount of information loss, ignoring higher-order neuronal interactions for decoding.

Firing Rate. To calculate firing rates, time was divided into $dt = 1$ ms bins, and a binary spike train, ρ_i was created for each neuron, i, equal to 1 if there was a spike in $(t, t + dt)$, and 0 otherwise in units of spk/s.

Spike-Count Correlation. The spike-count correlations between neurons i and j were calculated using the standard correlation coefficient, r, calculated as

$$r(\rho_i(t), \rho_j(t)) = \frac{Cov\left(\rho_i(t), \rho_j(t)\right)}{\sqrt{Var\left(\rho_i(t)\right) Var\left(\rho_j(t)\right)}},$$

where $Cov\left(\rho_i(t), \rho_j(t)\right)$ is the covariance between the spike-counts of the two neurons $Cov\left(\rho_i(t), \rho_j(t)\right) = \left\langle \left(\rho_i(t) - \left\langle \left(\rho_i(t)\right)\right\rangle\right)\left(\rho_j(t) - \left\langle \left(\rho_j(t)\right)\right\rangle\right)\right\rangle$, where $\left\langle \left(\rho_i(t)\right)\right\rangle$ denotes the temporal average $\langle(\rho_i(t))\rangle = \frac{1}{T}\sum_{t=1}^{T} \rho_i(t)$.

Sequential State Correlation. The sequential state correlation is the correlation across all sequential states, $r(s(t), s(t + dt))$, where a state, $s(t)$, is the sequence of neurons active at timestep t and $dt = 1$ (as above). This measure reflects the similarity of sequential activation patterns. Consistent $r(s(t), s(t + dt))$ of unity indicates robust neuronal ensembles, whereas $r(s(t), s(t + dt)) \sim 0$ suggests independent neuronal activity.

Spatial Correlation Decay. The spatial correlation decay rate, ξ, is estimated by fitting an exponential to the spike-count correlation vs. neuronal distance, d, (calculated as) for each simulation:

$$r(d) = e^{\frac{-d}{\xi}},$$

where d is calculated on the spatial grid with unit distance between neighboring cells.

Susceptibility. Susceptibility, χ_ρ (69), is a signature of criticality that can be calculated as

$$\chi_\rho = \left\langle \rho_S^2 \right\rangle - \langle \rho_S \rangle^2,$$

where $\rho_S = \frac{1}{N}\sum_i \rho_i$ is the population spiking activity order parameter (46).

Metastability. Metastability (70), χ_θ, measures the variability in the phase alignment order parameter between each neuron calculated as

$$\chi_\theta = N\left(\left\langle \theta^2 \right\rangle - \langle \theta \rangle^2\right),$$

where $\theta = \frac{1}{N}\sum_i e^{i\theta_i}$ is the phase alignment order parameter between each neuron with θ_i estimated from the firing rate using the Hilbert transform.

Communicability. Communicability, $C = \frac{1}{N^2}\sum_{i,j} e^{W_{i,j}}$, where $W_{i,j}$ is the normalized weighted connectivity matrix estimated using the functional connectivity $W_{i,j} = r_{i,j} / \left(\sqrt{r_i}\sqrt{r_j}\right)$ from the neuronal pairwise correlation matrix $r_{i,j}$ and the neuron strength $\sqrt{r_i} = \sum_j r_{i,j}$. Communicability addresses the fact that despite two neurons not possessing a direct functional connection, if they share many neighboring functional connections, they should be regarded as closer together than the two weakly correlated neurons that can only be joined through a long chain of neurons.

Data, Materials, and Software Availability. All code required to reproduce the results in the main text are available on GitHub (www.github.com/Bmunn/Layer5_Arousal) (71).

Author affiliations: [a]Brain and Mind Centre, School of Medical Sciences, Faculty of Medicine and Health, University of Sydney, Sydney 2050, Australia; [b]Complex Systems, School of Physics, Faculty of Science, University of Sydney, Sydney 2050, Australia; [c]Institute of Computer Science, University of Tartu, Tartu 51009, Estonia; [d]Institute of Biology, Humboldt University of Berlin, Berlin 10099, Germany; and [e]NeuroCure Center of Excellence, Charité Universitätsmedizin Berlin, Berlin 10099, Germany

1. G. Tononi, M. Boly, M. Massimini, C. Koch, Integrated information theory: From consciousness to its physical substrate. *Nat. Rev. Neurosci.* **17**, 450–461 (2016).
2. S. Dehaene, L. Naccache, Towards a cognitive neuroscience of consciousness: Basic evidence and a workspace framework. *Cognition* **79**, 1–37 (2001).
3. R. Llinás, U. Ribary, D. Contreras, C. Pedroarena, The neuronal basis for consciousness. *Philos. Trans. R Soc. Lond B Biol. Sci.* **353**, 1841–1849 (1998).
4. E. Tagliazucchi, P. Balenzuela, D. Fraiman, D. R. Chialvo, Criticality in large-scale brain FMRI dynamics unveiled by a novel point process analysis. *Front. Physiol.* **3**, 15 (2012).
5. L. Cocchi, L. L. Gollo, A. Zalesky, M. Breakspear, Criticality in the brain: A synthesis of neurobiology, models and cognition. *Prog. Neurobiol.* **158**, 132–152 (2017).
6. E. J. Müller, B. Munn, J. M. Shine, Diffuse neural coupling mediates complex network dynamics through the formation of quasi-critical brain states. *Nat. Commun.* **11**, 6337 (2020), 10.1101/2020.06.09.141416.
7. A. K. Seth, T. Bayne, Theories of consciousness. *Nat. Rev. Neurosci.* **23**, 439–452 (2022).
8. G. M. Edelman, Naturalizing consciousness: A theoretical framework. *Proc. Natl. Acad. Sci. U.S.A.* **100**, 5520–5524 (2003).
9. S. Dehaene, J. P. Changeux, L. Naccache, Conscious, preconscious, and subliminal processing: A testable taxonomy. *Trends Cogn. Sci.* **10**, 204–211 (2006).
10. B. J. Baars, Global workspace theory of consciousness: Toward a cognitive neuroscience of human experience. *Prog. Brain Res.* **150**, 45–53 (2005).
11. W. A. Phillips, T. Bachmann, J. F. Storm, Apical function in neocortical pyramidal cells: A common pathway by which general anesthetics can affect mental state. *Front. Neural Circuits* **12**, 50 (2018).
12. G. Tononi, Consciousness and complexity. *Science* **282**, 1846–1851 (1998).
13. S. Laureys *et al.*, Restoration of thalamocortical connectivity after recovery from persistent vegetative state. *Lancet* **355**, 1790–1791 (2000).
14. S. M. Sherman, R. W. Guillery, Functional organization of thalamocortical relays. *J. Neurophysiol.* **76**, 1367–1395 (1996).

15. E. G. Jones, Viewpoint: The core and matrix of thalamic organization. *Neuroscience* **85**, 331–345 (1998).
16. M. Oizumi, S. Amari, T. Yanagawa, N. Fujii, N. Tsuchiya, Measuring integrated information from the decoding perspective. *PLoS Comput. Biol.* **12**, e1004654 (2016).
17. P. Anderson, More is different. *Science* **177**, 393–396 (1972).
18. J. Aru, M. Suzuki, M. E. Larkum, Cellular mechanisms of conscious processing. *Trends Cogn. Sci.* **24**, 814–825 (2020).
19. T. Bachmann, M. Suzuki, J. Aru, Dendritic integration theory: A thalamo-cortical theory of state and content of consciousness. *PhiMiSci* **1** (2020). https://doi.org/10.33735/phimisci.2020.II.52.
20. S. Ramaswamy, H. Markram, Anatomy and physiology of the thick-tufted layer 5 pyramidal neuron. *Front. Cell. Neurosci.* **9**, 233 (2015).
21. M. E. Larkum, J. J. Zhu, B. Sakmann, A new cellular mechanism for coupling inputs arriving at different cortical layers. *Nature* **398**, 338–341 (1999).
22. M. Larkum, A cellular mechanism for cortical associations: An organizing principle for the cerebral cortex. *Trends Neurosci.* **36**, 141–151 (2013).
23. M. Suzuki, M. E. Larkum, General anesthesia decouples cortical pyramidal neurons. *Cell* **180**, 666–676.e13 (2020).
24. N. Takahashi *et al.*, Active dendritic currents gate descending cortical outputs in perception. *Nat. Neurosci.* **23**, 1277–1285 (2020), 10.1038/s41593-020-0677-8.
25. E. G. Jones, The thalamic matrix and thalamocortical synchrony. *Trends Neurosci.* **24**, 595–601 (2001).
26. S. Dehaene, M. Kerszberg, J.-P. Changeux, A neuronal model of a global workspace in effortful cognitive tasks. *Proc. Natl. Acad. Sci. U.S.A.* **95**, 14529–14534 (1998).
27. G. M. G. Shepherd, N. Yamawaki, Untangling the cortico-thalamo-cortical loop: Cellular pieces of a knotty circuit puzzle. *Nat. Rev. Neurosci.* **22**, 389–406 (2021), 10.1038/s41583-021-00459-3.
28. J. M. Shine, The thalamus integrates the macrosystems of the brain to facilitate complex, adaptive brain network dynamics. *Prog. Neurobiol.* **199**, 101951 (2020).
29. F. Clascá, P. Rubio-Garrido, D. Jabaudon, Unveiling the diversity of thalamocortical neuron subtypes. *Eur. J. Neurosci.* **35**, 1524–1532 (2012).
30. M. J. Redinbaugh *et al.*, Thalamus modulates consciousness via layer-specific control of cortex. *Neuron* **106**, 66–75.e12 (2020).
31. J. Tasserie *et al.*, Deep brain stimulation of the thalamus restores signatures of consciousness in a nonhuman primate model. *Sci. Adv.* **8**, eabl5547 (2022).
32. J. M. Shine *et al.*, Computational models link cellular mechanisms of neuromodulation to large-scale neural dynamics. *Nat. Neurosci.* **24**, 765–776 (2021).
33. E. Hay, S. Hill, F. Schürmann, H. Markram, I. Segev, Models of neocortical layer 5b pyramidal cells capturing a wide range of dendritic and perisomatic active properties. *PLoS Comput. Biol.* **7**, e1002107 (2011).
34. A. S. Shai, C. A. Anastassiou, M. E. Larkum, C. Koch, Physiology of layer 5 pyramidal neurons in mouse primary visual cortex: Coincidence detection through bursting. *PLoS Comput. Biol.* **11**, e1004090 (2015).
35. E. M. Izhikevich, Spike-timing dynamics of neuronal groups. *Cereb. Cortex* **14**, 933–944 (2004).
36. A. S. Ecker *et al.*, Decorrelated neuronal firing in cortical microcircuits. *Science* **327**, 584–587 (2010).
37. A. N. Burkitt, A review of the integrate-and-fire neuron model: II. Inhomogeneous synaptic input and network properties. *Biol. Cybern.* **95**, 97–112 (2006).
38. M. Breakspear, Dynamic models of large-scale brain activity. *Nat. Neurosci.* **20**, 340–352 (2017).
39. E. M. Izhikevich, Which model to use for cortical spiking neurons? *IEEE Trans. Neural Netw.* **15**, 1063–1070 (2004).
40. J. W. Phillips *et al.*, A repeated molecular architecture across thalamic pathways. *Nat. Neurosci.* **22**, 1925–1935 (2019).
41. M. T. Alkire, A. G. Hudetz, G. Tononi, Consciousness and anesthesia. *Science* **322**, 876–880 (2008).
42. A. Renart *et al.*, The asynchronous state in cortical circuits. *Science* **327**, 587–590 (2010).
43. M. A. Muñoz, Colloquium: Criticality and dynamical scaling in living systems. *Rev. Mod. Phys.* **90**, 031001 (2018).
44. W. L. Shew *et al.*, Adaptation to sensory input tunes visual cortex to criticality. *Nat. Phys.* **11**, 659–663 (2015).
45. M. A. Smith, A. Kohn, Spatial and temporal scales of neuronal correlation in primary visual cortex. *J. Neurosci.* **28**, 12591–12603 (2008).
46. R. V. Williams-García, M. Moore, J. M. Beggs, G. Ortiz, Quasicritical brain dynamics on a nonequilibrium Widom line. *Phys. Rev. E* **90**, 062714 (2014).
47. M. I. Rabinovich, R. Huerta, P. Varona, V. S. Afraimovich, Transient cognitive dynamics, metastability, and decision making. *PLoS Comput. Biol.* **4**, e1000072 (2008).
48. E. Estrada, N. Hatano, Communicability in complex networks. *Phys. Rev. E* **77**, 036111 (2008).
49. J. J. Crofts, D. J. Higham, A weighted communicability measure applied to complex brain networks. *J. R. Soc. Interface* **6**, 411–414 (2009).
50. J. Wilting, V. Priesemann, Between perfectly critical and fully irregular: A reverberating model captures and predicts cortical spike propagation. *Cereb. Cortex* **29**, 2759–2770 (2019).
51. S. Dehaene, J.-P. Changeux, Experimental and theoretical approaches to conscious processing. *Neuron* **70**, 200–227 (2011).
52. G. Tononi, O. Sporns, G. M. Edelman, A measure for brain complexity: Relating functional segregation and integration in the nervous system. *Proc. Natl. Acad. Sci. U.S.A.* **91**, 5033–5037 (1994).
53. A. Palmigiano, T. Geisel, F. Wolf, D. Battaglia, Flexible information routing by transient synchrony. *Nat. Neurosci.* **20**, 1014–1022 (2017).
54. J. Aru, M. Suzuki, R. Rutiku, M. E. Larkum, T. Bachmann, Coupling the state and contents of consciousness. *Front. Syst. Neurosci.* **13**, 43 (2019).
55. T. A. Zolnik *et al.*, Layer 6b is driven by intracortical long-range projection neurons. *Cell Rep.* **30**, 3492–3505.e5 (2020).
56. C. Labarrera *et al.*, Adrenergic modulation regulates the dendritic excitability of layer 5 pyramidal neurons in vivo. *Cell Rep.* **23**, 1034–1044 (2018).
57. J. M. Shine, Neuromodulatory control of complex adaptive dynamics in the brain. *Interface Focus.* **13**, 20220079 (2023).
58. D. A. Pinotsis, G. Fridman, E. K. Miller, Cytoelectric coupling: Electric fields sculpt neural activity and "tune" the brain's infrastructure. *Prog. Neurobiol.* **226**, 102465 (2023).
59. E. M. Izhikevich, Simple model of spiking neurons. *IEEE Trans. Neural Netw.* **14**, 1569–1572 (2003).
60. E. M. Izhikevich, *Dynamical Systems in Neuroscience* (MIT press, 2007).
61. R. Pauli, P. Weidel, S. Kunkel, A. Morrison, Reproducing polychronization: A guide to maximizing the reproducibility of spiking network models. *Front. Neuroinform.* **12**, 46 (2018).
62. M. Hopkins, S. Furber, Accuracy and efficiency in fixed-point neural ODE solvers. *Neural Comput.* **27**, 2148–2182 (2015).
63. R. Brette *et al.*, Simulation of networks of spiking neurons: A review of tools and strategies. *J. Comput. Neurosci.* **23**, 349–398 (2007).
64. J. Szentágothai, The 'module-concept' in cerebral cortex architecture. *Brain Res.* **95**, 475–496 (1975).
65. S. Heitmann, T. Boonstra, M. Breakspear, A dendritic mechanism for decoding traveling waves: Principles and applications to motor cortex. *PLoS Comput. Biol.* **9**, e1003260 (2013).
66. D. Ledergerber, M. E. Larkum, The time window for generation of dendritic spikes by coincidence of action potentials and EPSPs is layer specific in somatosensory cortex. *PLoS One* **7**, e33146 (2012).
67. C. Wahl-Schott, M. Biel, HCN channels: Structure, cellular regulation and physiological function. *Cell. Mol. Life Sci.* **66**, 470–494 (2009).
68. A. Levina, V. Priesemann, J. Zierenberg, Tackling the subsampling problem to infer collective properties from limited data. *Nat. Rev. Phys.* **4**, 770–784 (2022).
69. P. Moretti, M. A. Muñoz, Griffiths phases and the stretching of criticality in brain networks. *Nat. Commun.* **4**, 2521 (2013).
70. G. Deco, M. L. Kringelbach, V. K. Jirsa, P. Ritter, The dynamics of resting fluctuations in the brain: Metastability and its dynamical cortical core. *Sci. Rep.* **7**, 3095 (2017).
71. B. Munn, Layer5_Arousal. Github. https://github.com/Bmunn/Layer5_Arousal. Deposited 28 September 2023.